



## A Coupled Rigid-viscoplastic Numerical Modeling for Evaluating Effects of Shoulder Geometry on Friction Stir-welded Aluminum Alloys

J. Fabregas Villegas<sup>a</sup>, A. Martínez Guarín<sup>b</sup>, J. Unfried-Silgado<sup>\*b</sup>

<sup>a</sup> Departamento de Ingeniería mecánica, Grupo IMTEF, Universidad Autónoma del Caribe, Barranquilla, Colombia

<sup>b</sup> Departamento de Ingeniería mecánica, Grupo ICT, Universidad de Córdoba, Montería, Colombia

### PAPER INFO

#### Paper history:

Received 24 August 2018

Received in revised form 28 October 2018

Accepted 03 January 2019

#### Keywords:

Friction Stir Welding

Finite Element Model

Aluminum Alloy

Heat Generation

Plasticity

### ABSTRACT

Shoulder geometry of tool plays an important role in friction-stir welding because it controls thermal interactions and heat generation. This work is proposed and developed a coupled rigid-viscoplastic numerical modeling based on computational fluid dynamics and finite element calculations aiming to understand these interactions. Model solves mass conservation, momentum, and energy equations in three dimensions, using appropriate boundary conditions, considering mass flow as a non-Newtonian, incompressible, viscoplastic material. Boundary conditions of heat transfer and material flow were determined using a sticking/sliding contact condition at tool / workpiece interface. Thermal history, as well as shear stress and rotational speed fields, forces and torque values for three shoulder geometry conditions were calculated. Numerical results of thermal history, torque and forces during welding showed good correlation with experimentally measured data.

doi: 10.5829/ije.2019.32.02b.17

## 1. INTRODUCTION

Friction stir welding (FSW) is a solid state joining process invented and patented in The Welding Institute (TWI) in 1991 [1]. During FSW process a rotating tool (outfitted with a pin and a shoulder) is inserted into plates to be joined. Initially, a non-consumable tool rotating with a constant rotation speed ( $\omega$ ) is pushed down with an axial force ( $F_z$ ) and inserted orthogonally into the joint line, until shoulder gets contact to the surface of plates. Interactions during contact among shoulder, pin and welded surface generate sufficient heat for softening, plastically deforming, and stirring the welded material. Bead of welding is completed when rotating tool is travelling along the joint line with a constant traveled or traverse speed [2]. Microstructural zones produced during FSW consist in a central region named stir zone (SZ), which contents nugget region, thermomechanical affected zone (TMAZ) and heat affected zone (HAZ), whose particular characteristics depend on, mostly, of tool rotation velocity vector. Side where tool rotational speed

vector is the same to traveled speed vector is named advancing side (AS), whilst on the other side, when the same vectors are opposite, is named retreating side (RS) [3]. FSW parameters, such as, rotational speed ( $\omega$ ), traveled speed ( $v_s$ ), torque ( $\tau$ ), and downward force ( $F_z$ ) are very important, because they define energy consumption by process, mechanical properties, quality, and performance of welded joints all of them related to heat generation [4-8], as shown in Figure 1.

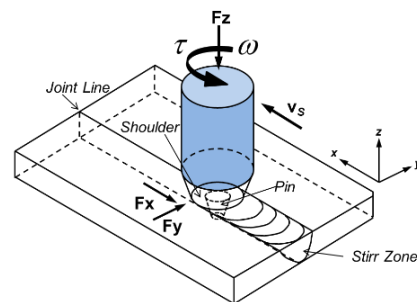


Figure 1. FSW regions, geometry and parameters

\*Corresponding Author Email: jimyunfried@correo.unicordoba.edu.co (J. Unfried-Silgado)

Welded joints quality in FSW has a strong dependence of heat generation during the process [9]. Thermal cycles affect plastic flow, whereas peaks of temperature control the recrystallization mechanism [10-12]. On the other hand, several works have proved that heat generation in FSW is very sensible to geometry of tool together with process parameters [13-15]. Traditionally, experimental measurements have been used to study thermal processes in FSW. However, setup limitations, costs, and difficulties to determine entire field of temperatures, affecting an effective understanding of heat generation during the process. Numerical modeling is an invaluable alternative to solve problems aiming to understand thermal process and heat generation, and material flow during FSW [16-18].

Several works have been carried out to explore by means of numerical modeling simulation, aiming to approach and understand, simultaneously, the heat generation, flow material and mechanical behavior in FSW joints. Different works based on finite elements (FE) modeling have been studied [19-29]. Some FE models are based on thermomechanical effects and its relationships with process parameters, combined with viscoplastic effects, energy and mass conservation equations. Further, these models incorporate tool geometry and base materials characteristics. FE models have disadvantage to demand a lot of time and computational processing data resources. On the other hand, several works have used models based on computational fluid dynamics (CFD) [29-40]. CFD models are complemented with thermomechanical 3-D plastic flow, Carreau's model for viscoplastic effect, Zenner-Holloman equations, among others. The most important advantages using CFD modeling are: to obtain significant asymmetry in both metal flow and temperature fields, additionally it can be observed that the plastic flow is significantly affected by heat transport within the workpiece, the effects of thermal history on residual stress, to obtain more realistic parameters analyses between numerical modeling with statistical optimization, predict the process variables, material flow pattern and grain size in the welded joints, to predict conditions that result in defect generation during friction stir welding.

Recently, it has been developed a meshless particle method for the analysis of transient heat transfer during FSW process [40]. The model was validated with experimental data from FSW of Al6061-T6 to predict the maximum temperature, heat generation rate and torque for various welding parameters and tool dimensions. Meshless and implicit FE simulations obtained yield similar results, but the former can save a lot of computational time. Other works have been oriented to use analytical models to estimate heat generation of FSW in several aluminum alloys [38]. These models involve taper cylindrical pin profile, varying process conditions and sizes of tool geometry. Results were compared to experimentally approach of literature, obtaining good

agreement between model and experimental data. Other simulations used a one-dimensional heat transfer model, a cylindrical pin tool, and an alternative heat index (AHI), aiming to analyze the effects of heat generation from welding parameters to maintain a constant shear surface temperature during FSW of AA2024 aluminum alloy [39]. Finally, other works used a coupled thermo-mechanical problem with an enhanced friction model to include the effect of non-uniform pressure distribution under the pin shoulder during FSW processes using threaded cylindrical pin tools [41]. Moreover, a complete numerical model based on CFD was used to simulate material flow and heat transfer in friction stir processing in steel pipelines [42], which was successful to correlate peak temperatures with experimental data.

The aforementioned works showed the progress in numerical modeling, aiming to quantitative understanding of FSW process. However, despite of, precision and high quality of obtained results, it still has not been implemented a modeling that show directly relationships between parameters and tool geometry variations. In this sense, the goal of this work is to develop a coupled rigid-viscoplastic numerical modeling based on CFD simulation and FE numerical modeling calculations. The model aiming to calculate the effects of variation in shoulder geometry of tool on thermal history (peak temperatures and thermal cycles) and process parameters (rotational speed and torque) during friction-stir welding of AA1100 aluminum alloys plates.

## 2. NUMERICAL SIMULATION

A computational fluid dynamics (CFD) three-dimensional modeling coupled to viscoplastic-rigid equations was performed using finite element (FE) commercial software ANSYS®. In the following sections are described the mathematical and simulation conditions.

**2.1. Mathematical Models** This work is assumed that the material during FSW process have an incompressible single-phase fluid behavior. The model of continuity is used for describing incompressible flow, which is shown in Equation (1) and momentum conservation for the continuity model is represented by Equation (2).

$$\frac{\partial u_i}{\partial x_i} = 0 \quad (1)$$

$$\rho \frac{\partial u_i u_j}{\partial x_i} = -\frac{\partial P}{\partial x_i} + \frac{\partial}{\partial x_i} \left( \mu \frac{\partial u_j}{\partial x_i} + \mu \frac{\partial u_i}{\partial x_j} \right) - \rho v \frac{\partial u_j}{\partial x_j} \quad (2)$$

where  $\rho$  is density,  $u$  is velocity of viscoplastic flow,  $P$  is pressure,  $\mu$  is viscosity for non-Newtonian flow,  $v$  is velocity, and  $x$  represents the longitudinal coordinate of the welded joint.

Equation (3) was used to represent the energy conservation for the conduction heat transfer by diffusion of species, viscous dissipation and chemical reactions, if any. Where  $\rho$  is density,  $u$  is velocity of viscoplastic flow,  $P$  is pressure,  $\mu$  is viscosity for non-Newtonian flow,  $v$  is velocity,  $E$  is energy,  $T$  is temperature,  $h$  is sensible enthalpy,  $J$  is the diffusion flux of species  $j$ ,  $S_k$  is the heat of chemical reaction,  $k_{eff}$  is the effective conductivity, and  $\bar{\tau}_{eff}$  is the deviatoric stress tensor.

$$\frac{\partial}{\partial t}(\rho E) + \nabla v(\rho E + P) = \nabla[(k_{eff} \nabla T) - \sum_j h_j J_j + (\bar{\tau}_{eff} v)] + S_k \quad (3)$$

Aiming to model the FSW processing have been used Equations (4) to (8). The Zener – Hollomon model are showed in Equations (4) and (5). Room temperature is considered as 298 K (25°C).

$$Z = \dot{\varepsilon} \cdot e^{\frac{Q}{RT}} \quad (4)$$

$$\dot{\varepsilon} = \left\{ \frac{2}{3} \left[ \frac{\partial u_i}{\partial x_j} + \frac{\partial u_j}{\partial x_i} \right] \right\} \left[ \frac{1}{2} \left( \frac{\partial u_i}{\partial x_j} + \frac{\partial u_j}{\partial x_i} \right) \right]^{1/2} \quad (5)$$

where  $Q$  is the activation energy,  $R$  is the universal gas constant,  $T$  is the temperature of activation,  $\dot{\varepsilon}$  is the rate effective strain,  $u$  is velocity of viscoplastic flow, and  $x$  represents the longitudinal coordinate of the welded joint. Equation (6) represents the flow stress.

$$\sigma_e = \frac{1}{\alpha} \sinh^{-1} \left[ \left( \frac{Z}{A} \right)^{1/n} \right] \quad (6)$$

where terms  $\alpha$ ,  $A$ , and  $n$ , are specific constants, which depend on manufacturing process of material, whereas,  $Z$  value is given by Equation (4). Viscosity can be determined from flow stress and effective strain rate, in accordance to Carreau's expressions for viscoplastic model, which are shown in Equations (7) and (8).

$$\mu = \frac{\sigma_e}{3\dot{\varepsilon}} \quad (7)$$

$$\mu = H(T) \left[ \mu_\infty + (\mu_0 + \mu_\infty)(1 + \gamma^2 \lambda^2)^{(n-1)/2} \right] \quad (8)$$

where  $\lambda$  is a time constant,  $\gamma$  is shear rate,  $\mu_0$  and  $\mu_\infty$  are, upper and lower limiting values of the fluid viscosity, respectively, and  $H(T)$  is the total enthalpy for temperature dependence. The variable  $n$  for non-Newtonians flow, is defined in accordance to material type. Range of values are  $n = 1$  for Newtonian fluid;  $n > 1$  for Dilatant fluids, and  $n < 1$  for Pseudo-plastics fluids.

## 2. 2. Heat Generation and Boundary Conditions

Geometry and initial conditions used to describe the frictional heat generation  $Q$  in the interface tool/plate are shown in Figure 2 and Equation (9).

$$\dot{Q}_{total} = \frac{2}{3} \pi \omega \tau_{contact} \left[ \begin{aligned} &(R_H^3 - R_{bp}^3) + \\ &\left[ \left( \frac{3}{4} \frac{H}{\cos \beta} \right) (2R_{bp} - H \tan \beta)^2 \right] \\ &+ (R_{bp} - H \tan \beta)^3 \end{aligned} \right] \quad (9)$$

where  $\omega$  is rotational speed,  $H$  is height of pin,  $R_H$  is shoulder radius,  $R_{bp}$  is pin base radius,  $R_p$  is pin radius,  $\beta$  is the conicity angle,  $\tau_{contact}$  is shear stress. Equation (10) describes the heat dissipation of the plate with bottom and surroundings, when all of them terms have been explained before.

$$-k \frac{\partial T}{\partial z} = h(T - T_\infty) + \sigma \varepsilon (T^4 - T_\infty^4) \quad (10)$$

Aiming to calculate the value of torque, it has been used the standard function of calculator tool available in the software, which allows to determine the torque of a boundary section in a specific axis. This torque function has the same behavior that force function, which is defined as the force due to pressure plus the force due to the mass flow (owing to advection of momentum). If there is wall cut data in the results file, the viscous force is added to the calculated force function.

During FSW, the conduction heat transfer has been transformed in the convective heat transfer by the Newton's cooling law and radiations heat transfer, respectively. In Equation (10),  $h$  is the convection heat transfer coefficient,  $\sigma$  is the constant of Stefan-Boltzmann,  $\varepsilon$  is the emissivity. The thermal conductivity  $k$  for aluminum alloy AA1100 in function of temperature  $T$  and specific heat  $C_p$  are represented through Equations (11) and (12), respectively.

$$k = -1.30739 \times 10^{-6} T^3 + 3.03745 \times 10^{-3} T^2 - 2.29503 T + 796.793 \quad (11)$$

$$C_p = 6.0519 \times 10^{-6} T^3 - 1.45290 \times 10^{-2} T^2 + 11.711 T - 2163.88 \quad (12)$$

## 3. MATERIALS AND PROCESS PARAMETERS

**3.1. Base Metal** Plates of 240 mm x 140 mm and 6 mm of thickness of Aluminum alloy AA1100 in strain-

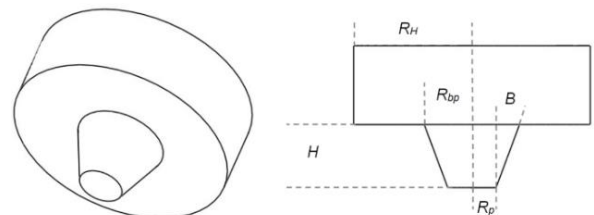


Figure 2. Tool measures

hardened condition were used as base material. Chemical composition and mechanical properties of base metal are shown in Table 1 and Table 2, respectively.

**3. 2. Tool Geometry**

Three different monolithic tools made in AISI/SAE H-13 steel have been fabricated with identical dimensions and geometry, with threaded conical pin, but different shoulder geometry. Figure 3 shows dimensional and geometry characteristics of shoulder tools, which correspond to featured shoulder tool with spiral and concentric circles, and a flat shoulder. In accordance to Figure 2, the most important dimensions and geometrical characteristics of tools used in this investigation are shown in Table 3. Chemical composition of AISI H13 steel used to fabricate FSW tools is shown in Table 4.

**3. 3. Experimental Setup**

Welded joints of AA1100 plates were developed in butt position using a vertical milling machine with 3.5 HP. Plates were firmly gripped to bench using clamps. Welded joints were carried out using the process parameters shown in Table 5. These same parameters were used for all types of shoulder geometry of studied tools. The FSW influence on microstructure and mechanical properties of the welded joints had been explored in other previous work, as well as, thermocouples and thermal cycles distribution [43].

**3. 4. Geometry and Mesh of the System**

Geometrical set-up, mesh, boundary values and initial condition are shown in Figure 4 and Table 6. Coupling Multiphysics methods are used to model the interaction

**TABLE 1.** Chemical composition of base material (wt%)

Al	Si + Fe	Cu	Mn	Be
Bal.	>0.10	0.05-0.20	>0.05	<0.0008

**TABLE 2.** Mechanical properties of base material

S <sub>V</sub> (MPa)	S <sub>U</sub> (MPa)	Elongation (%)	Hardness HV
25 - 40	75 - 105	35	45

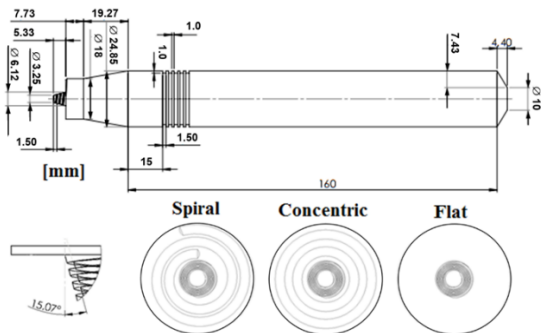


**Figure 3.** Profile of tools and shoulder's geometry

**TABLE 3.** Dimensions and shoulder characteristics

radius of shoulder R <sub>H</sub> [m]	Pin base radius R <sub>bp</sub> [m]	Pin radius R <sub>p</sub> [m]	Height of pin H [m]	Conicity angle β [°]
0.009	0.00306	0.001625	0.00533	15.07
Measured part/Shoulder geometry		Flat	Spiral	Concentric
Shoulder area (mm <sup>2</sup> )		225	309	273
width/deep ratio (mm/mm)		0 / 0	1 / 1.5	1 / 1

**TABLE 4.** Chemical composition of AISI H13 tool steel (wt%)

Fe	C	Cr	Mn	Si	V
Bal.	0.39	5.20	0.40	1.10	0.95

**TABLE 5.** FSW process parameters used to weld

Parameters	v <sub>s</sub> (mm.min <sup>-1</sup> )	ω (rpm)
values	100	1000

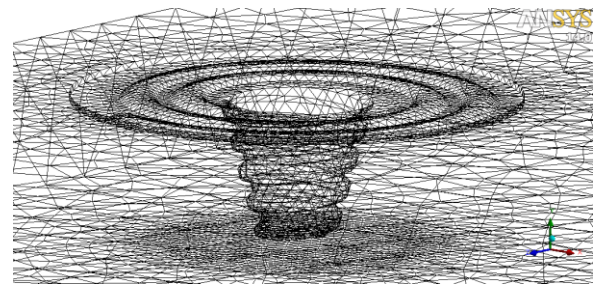


**Figure 4.** Volumetric mesh

**TABLE 6.** Volumetric mesh parameters

Type of Shoulder	Elements	Nodes	Type of Mesh
Flat	97398	21432	Tetrahedrons
Concentric	140138	29522	Tetrahedrons
Spiral	141335	29736	Tetrahedrons

of the tool with plates [44]. For numerical simulations were selected tetragonal elements type. These elements are compatible with remesh techniques used in this work, aiming to obtain maximum efficiency orthogonality during deformation. Both nodes and elements were tested until to obtain meshing independence. Figure 4 shows meshing of threaded profile and featured concentric shoulder tool before to realize the welded joint. Mesh-independence was calculated using meshing of 1.4x10<sup>-5</sup>, 2.9x10<sup>-5</sup> and 5.9x10<sup>-5</sup> elements, obtaining 0.36 and 0.016% of calculating error, respectively.

In order to simulate the viscoplastic state of the aluminum alloy, Carreau's model was applied through Equations (7) and (8), which required the assignment of

the volumetric deformation coefficients of the material. There were used the following values: time constant  $\lambda = 10$  s, constant  $n = 0.25$ , which was chosen for pseudoplastic fluid conditions and viscosity values where the material shows its greater solidity  $\mu_{\infty} = 1e^{+07}$  kg.ms<sup>-1</sup> and the minimum value of viscosity where the material obtains its greater fluidity in plastic state  $\mu_0 = 0$  kg.ms<sup>-1</sup>. Interaction between process parameters and coupled modeling allows establishing relationships among values of functions and process parameters values: Torque, shear stress, heat flow, mechanical power and efficiency. Finally, it was compared the experimentally obtained measurements based on previous work [43] and numerical modeling results, regarding values from thermal cycles (peak of temperatures and cooling rates), torque, heat flow and process efficiency.

**4. RESULTS AND DISCUSSION**

**4. 1. Thermomechanical Simulation Analysis**

Figure 5 shows the distribution of temperature during thermal transient state in longitudinal section of welding plate for two different times 10 and 22 s. It was noticed that in the contact zone between pin / plate, the remesh efficiency was not lost when the tool advances through the joint, which was observed for all shoulders profiles of the tools employed. It was observed that the temperatures field is heterogeneously distributed below of tool shoulder, which is due to non-asymmetric flow of material during FSW [45]. As it was expected, the highest temperatures are distributed around the interface pin/plate. Maximum value of temperature at the interface is 795 K (522°C), whereas at region away 10 mm from interface,

it is reached 689 K (416°C) of maximum temperature. Asymmetrical thermal contribution during FSW is well known and this is attributed to additive contribution of velocity fields at advancing side compared to retreating side [43, 45].

Figure 6 and Figure 7 show the results of the dynamic viscosity and tangential speed (velocity) fields at the contact area, including the interface pin tool / plate, respectively. Figure 6 shows by means of color mapping distribution the difference between viscosity behavior on and off region under shoulder of the tool, displaying fluidity (blue region) and solidity (red region), respectively. Calculated values are coherent with those observed in other works [46-49]. Maximum tangential speed in the stir zone (SZ) cannot exceed a determined value, which is given by product between angular speed and radius of shoulder of tool. Therefore, Figure 7 was used to validate the continuity of the system, showing that obtained range of values for velocity field is between 0.9 m. s<sup>-1</sup> until 8.9 m. s<sup>-1</sup>. There is a relationship between both aforementioned variables, since the higher stirring on the top surface, which is produced by higher tangential speed cause higher deformation of the material. Due to the above, strain is increased, and viscosity is decreased, as a result of the frictional heat generation during stir in the interface tool / plate. Shear stress is related to viscoplastic effect, such as is shown in Figure 8, proving the opposite relationship between this last and the dynamic viscosity field.

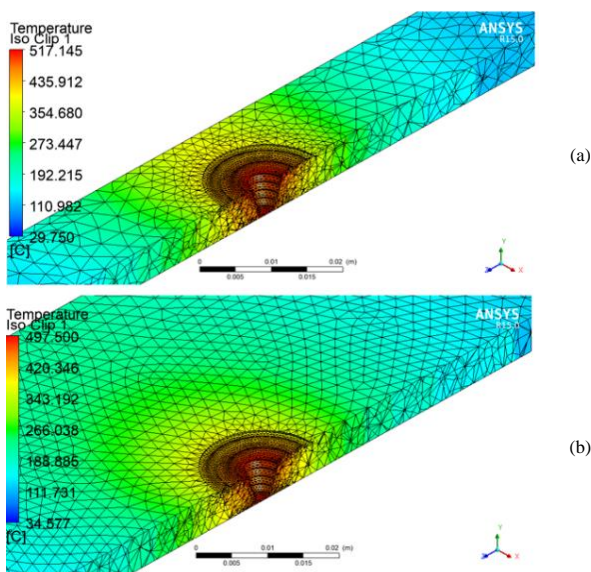


**Figure 5.** Temperature field in transient state (a) longitudinal (b) transversal section

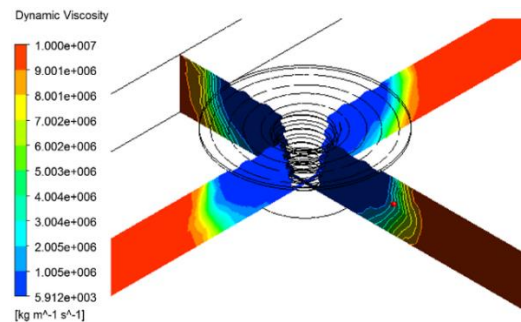


**Figure 6.** Dynamic viscosity behavior in the stir zone

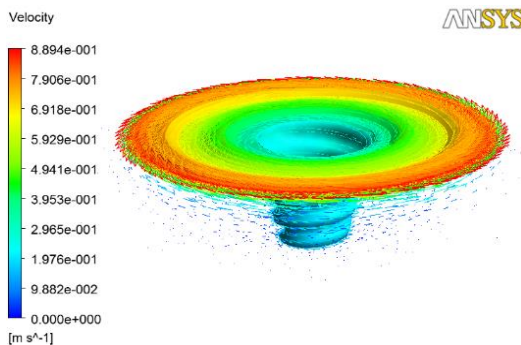


**Figure 7.** tangential speed field in the stir zone

**4. 2. Shear Stress and Torque Analysis** Figure 8 shows the shear stress field in the interface tool / plate, including shoulder and pin tool contact area. It can be observed that maximum value of Shear stress (11.8 MPa) agrees with location of maximum value of tangential speed (see Figure 7). The average values of shear stress for each type of evaluated tool is shown in Table 7. Maximum value of shear stress is for featured shoulder tool with spiral shape, which has the highest surface area of shoulder produced by higher relation width / deep of the groove in accordance to Table 3. Previous work has established that in stir zone (SZ) are achieved peak temperatures near to 80% of fusion temperature of base metal [47]. Aluminum alloy exhibits shear stress values between 10 to 15 MPa during high temperature deformation between 500 to 600 °C, respectively [50]. Numerical modelling results obtained in this work exhibit good correlation with experimental values above mentioned.

Using the obtained values by shear stress field it has been calculated the torque in function of time for each type of studied tools, consuming an elapsed time of 60 s, such as is shown in Figure 9. Table 8 shows the maximum value of torque obtained during stationary state of welding. There was no appreciable difference (<10%) between torque values in function of shoulder tool geometry. It is possible to explain this fact from heat distribution mechanisms in stir zone, which was discussed in previous work [43]. Additionally, calculated torque values are reasonable matched to other results obtained in other previous works that measured it experimentally, which were between 10 to 20 N.m [46, 51].

**4. 3. Microstructure Analysis and Thermal Cycles**

Figure 10 depicts a comparison among calculated isothermal distribution, experimentally observed microstructure, and respectively values of microhardness

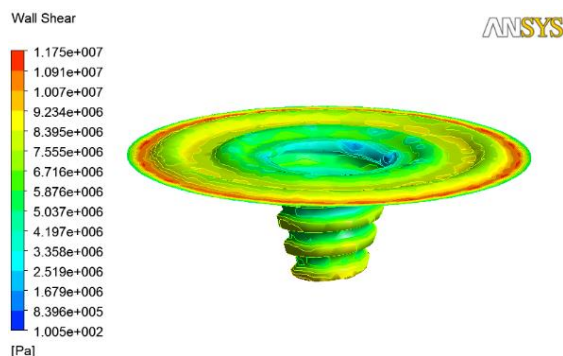


Figure 8. Shear stress in the interface pin tool/plate

TABLE 7. Average shear stress values calculated

Type of Shoulder	Flat	Spiral	Concentric
Shear stress [MPa]	7.82	8.16	8.11

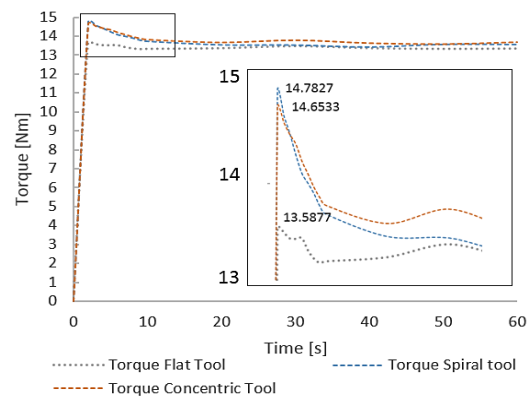


Figure 9. Analysis of torque values in function of time

TABLE 8. Maximum calculated torque value

Type of Shoulder	Flat	Spiral	Concentric
Torque [N.m]	13.6	14.8	14.7

measurements on a cross section of welded joint. It is observed a good correlation among behavior of hardness values and the different welding regions. An intensive reduction of hardness (approx. 50%) is observed covering regions located among heat affected zone (HAZ), thermomechanical affected zone (TMAZ), and stir zone (SZ). This hardness drops matches with isothermal regions that shows higher temperature just around interface tool / plate, exhibiting at the stir region (SZ) temperatures next to 767 K (494°C). Location of stir zone coincides with minimum value of viscosity, high and medium values of shear stress, and higher peak temperature, producing lower hardness and higher of grain size [43]. Increasing of viscosity, together with decreasing of shear stress and peaks of temperatures generate TMAZ and HAZ, respectively. In TMAZ due to combination of peak temperature and shear strength produce well known dynamic recrystallization process [43, 52].

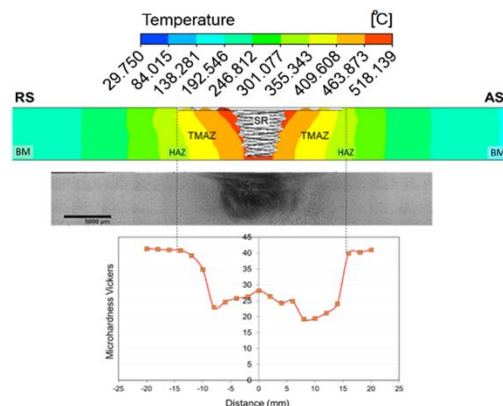


Figure 10. Microstructure, hardness and isothermal distribution of welded joint cross section

Isothermal distribution around stir zone has good correlation with shear stress field (Figure 8) and tangential speed field (Figure 7), through which is possible to explain the width of stir region, such as is observed in the microstructure of cross section of welded joint (Figure 10). Finally, thermal cycles for each type of shoulder tool were calculated in locations at 11 mm from welding line toward metal base, and which are shown in the Figure 11 and Figure 12, for advancing and retreating sides, respectively. It can be noticed the good correlation between experimental and simulation data. Calculated cooling rates are very similar for all cases of studied shoulder geometry tools and side of observation,  $5\text{ }^{\circ}\text{C}\cdot\text{s}^{-1}$  approximately. Experimentally obtained values reported in previous work in aluminum alloys is similar to those obtained in this work (between  $3$  and  $10\text{ }^{\circ}\text{C}\cdot\text{s}^{-1}$ ) [52]. Calculated thermal cycles were compared with experimentally measured thermal cycles obtained in a previous work under same conditions of process parameters during numerical simulation [43, 47]. A very good correlation between experimental and simulated values was observed. Peak temperatures in advanced side are higher than retreated side. This fact is consistent with the differences of vector contribution during FSW in both sides and lower hardness values observed in the advanced side [43, 47]. Differences between simulated and measured peak temperatures was less than 5%, which indicates acceptable accuracy of model presented in this work.

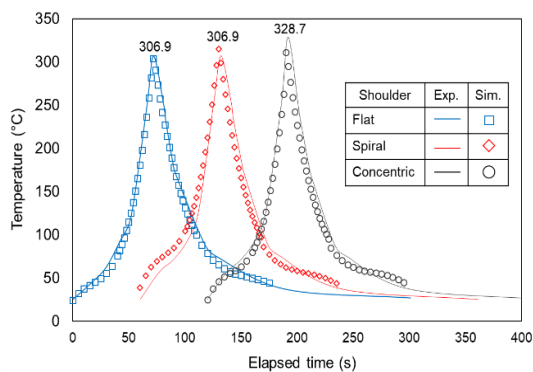


Figure 11. Thermal cycles in advanced side

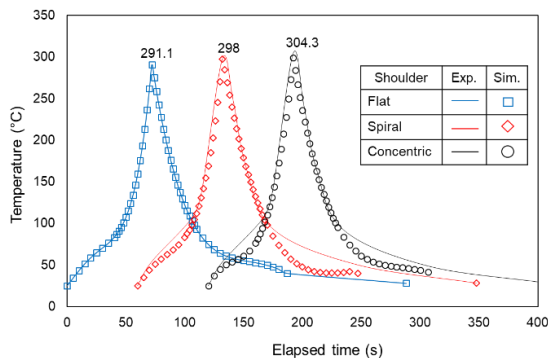


Figure 12. Thermal cycles in retreated side

## 5. CONCLUSIONS

A three-dimensional numerical simulation coupled to rigid-viscoplastic model was implemented in this work, which was successfully applied for simulated friction stir-welded joints of aluminum alloy AA1100 using three different tool geometries obtaining good accuracy.

Distribution of temperatures field obtained by numerical simulations correlate acceptably the behaviour during transient state and the heterogeneity distribution of temperatures below of tool shoulder for each shoulder geometry tool.

Tangential speed and shear stress fields for each type of shoulder tool geometry were calculated. Results were reasonably associated to plastic deformation (shear stress) and heat generation conditions (peak of temperatures) during FSW process, which were associated to shoulder tool type.

Shoulder flat geometry obtained lower peak temperature, torque, and shear stress values compared with spiral and circle concentric featured shoulder tools on evaluated conditions. These results were related to frictional behavior and area surface contact between tool and welded material.

## 6. REFERENCES

1. Thomas, W.M., "Friction stir welding", International Patent Application No. PCT/GB92/02203 and GB Patent Application No. 9125978.8, US Patent (5), (1991), 460-317.
2. Mishra, R.S., and Ma, Z.Y., "Friction stir welding and processing", *Materials Science and Engineering: R: Reports*, Vol. 50, No. 1–2, (2005), 1–78.
3. Rai, R., De, A., Bhadeshia, H.K.D.H., and DebRoy, T., "Friction stir welding tools", *Science and Technology of Welding and Joining*, Vol. 16, No. 4, (2011), 325–342.
4. Threadgill, P.L., Leonard, A.J., Shercliff, H.R., and Withers, P.J., "Friction stir welding of aluminium alloys", *International Materials Reviews*, Vol. 54, No. 2, (2009), 49–93.
5. Nandan, R., DebRoy, T., and Bhadeshia, H.K.D.H., "Recent advances in friction-stir welding – Process, weldment structure and properties", *Progress in Materials Science*, Vol. 53, No. 6, (2008), 980–1023.
6. Tanwar, P., and Kumar, V., "Friction Stir Welding: Review", *Science Technology & Engineering*, Vol. 3, No. 10, (2014), 172–176.
7. Zhang, Y.N., Cao, X., Larose, S., and Wanjara, P., "Review of tools for friction stir welding and processing", *Canadian Metallurgical Quarterly*, Vol. 51, No. 3, (2012), 250–261.
8. Lohwasser, D., and Chen, Z., *Friction stir welding: From basics to applications*, Elsevier, (2009).
9. Schmidt, H., and Hattel, J., "A local model for the thermomechanical conditions in friction stir welding", *Modelling and Simulation in Materials Science and Engineering*, Vol. 13, No. 1, (2005), 77–93.
10. Rajamanickam, N., Balusamy, V., Madhusudhana Reddy, G., and Natarajan, K., "Effect of process parameters on thermal history and mechanical properties of friction stir welds", *Materials & Design*, Vol. 30, No. 7, (2009), 2726–2731.

11. McNelley, T.R., Swaminathan, S., and Su, J.Q., "Recrystallization mechanisms during friction stir welding/processing of aluminum alloys", *Scripta Materialia*, Vol. 58, No. 5, (2008), 349–354.
12. Murr, L.E., Flores, R.D., Flores, O.V., McClure, J.C., Liu, G., and Brown, D., "Friction-stir welding: microstructural characterization", *Materials Research Innovations*, Vol. 1, No. 4, (1998), 211–223.
13. Colligan, K.J., "A conceptual model for the process variables related to heat generation in friction stir welding of aluminum", *Scripta Materialia*, Vol. 58, No. 5, (2008), 327–331.
14. Kumar, K., and Kailas, S. V., "The role of friction stir welding tool on material flow and weld formation", *Materials Science and Engineering: A*, Vol. 485, No. 1–2, (2008), 367–374.
15. Zhao, Y., Lin, S., Wu, L., and Qu, F., "The influence of pin geometry on bonding and mechanical properties in friction stir weld 2014 Al alloy", *Materials Letters*, Vol. 59, No. 23, (2005), 2948–2952.
16. Schmidt, H.B., and Hattel, J.H., "Thermal modelling of friction stir welding", *Scripta Materialia*, Vol. 58, No. 5, (2008), 332–337.
17. Ulysse, P., "Three-dimensional modeling of the friction stir-welding process", *International Journal of Machine Tools and Manufacture*, Vol. 42, No. 14, (2002), 1549–1557.
18. He, X., Gu, F., and Ball, A., "A review of numerical analysis of friction stir welding", *Progress in Materials Science*, Vol. 65, (2014), 1–66.
19. Chen, C.M., and Kovacevic, R., "Finite element modeling of friction stir welding—thermal and thermomechanical analysis", *International Journal of Machine Tools and Manufacture*, Vol. 43, No. 13, (2003), 1319–1326.
20. Buffa, G., Hua, J., Shivpuri, R., and Fratini, L., "Design of the friction stir welding tool using the continuum based FEM model", *Materials Science and Engineering: A*, Vol. 419, No. 1–2, (2006), 381–388.
21. Zhang, H.W., Zhang, Z., and Chen, J.T., "3D modeling of material flow in friction stir welding under different process parameters", *Journal of Materials Processing Technology*, Vol. 183, No. 1, (2007), 62–70.
22. Malik, V., Sanjeev, N.K., Hebbar, H.S., and Kailas, S. V., "Investigations on the Effect of Various Tool Pin Profiles in Friction Stir Welding Using Finite Element Simulations", *Procedia Engineering*, Vol. 97, (2014), 1060–1068.
23. Al-Badour, F., Merah, N., Shuaib, A., and Bazoune, A., "Coupled Eulerian Lagrangian finite element modeling of friction stir welding processes", *Journal of Materials Processing Technology*, Vol. 213, No. 8, (2013), 1433–1439.
24. Su, H., Wu, C.S., Bachmann, M., and Rethmeier, M., "Numerical modeling for the effect of pin profiles on thermal and material flow characteristics in friction stir welding", *Materials & Design*, Vol. 77, (2015), 114–125.
25. Grujcic, M., He, T., Arakere, G., Yalavarthy, H. V., Yen, C.F., and Cheeseman, B.A., "Fully coupled thermomechanical finite element analysis of material evolution during friction-stir welding of AA5083", *Proceedings of the Institution of Mechanical Engineers: Journal of Engineering Manufacture, Part B*, Vol. 224, No. 4, (2010), 609–625.
26. Chiumenti, M., Cervera, M., Agelet de Saracibar, C., and Dialami, N., "Numerical modeling of friction stir welding processes", *Computer Methods in Applied Mechanics and Engineering*, Vol. 254, (2013), 353–369.
27. Nandan, R., Roy, G.G., and Debroy, T., "Numerical simulation of three-dimensional heat transfer and plastic flow during friction stir welding", *Metallurgical and Materials Transactions A*, Vol. 37, No. 4, (2006), 1247–1259.
28. Mohan, R., Rajesh, N.R., and Kumar, S.S., "Finite element modeling for maximum temperature in friction stir welding of AA 1100 and optimization of process parameter by Taguchi Method", *IJRET: International Journal of Research in Engineering and Technology*, Vol. 3, No. 5, (2014), 728–733.
29. Nourani, M., Milani, A.S., and Yannacopoulos, S., "Taguchi optimization of process parameters in friction stir welding of 6061 aluminum alloy: A review and case study", *Engineering*, Vol. 3, No. 2, (2011), 144–155.
30. Colegrove, P.A., and Shercliff, H.R., "3-Dimensional CFD modelling of flow round a threaded friction stir welding tool profile", *Journal of Materials Processing Technology*, Vol. 169, No. 2, (2005), 320–327.
31. Atharifar, H., Lin, D., and Kovacevic, R., "Numerical and Experimental Investigations on the Loads Carried by the Tool During Friction Stir Welding", *Journal of Materials Engineering and Performance*, Vol. 18, No. 4, (2009), 339–350.
32. Hasan, A.F., Bennett, C.J., and Shipway, P.H., "A numerical comparison of the flow behaviour in Friction Stir Welding (FSW) using unworn and worn tool geometries", *Materials & Design*, Vol. 87, (2015), 1037–1046.
33. Roy, B., Medhi, T., and Saha, S.C., "Material flow modeling in friction stir welding of AA6061-T6 alloy and study of the effect of process parameters", *World Academy of Science, Engineering and Technology, International Journal of Environmental, Chemical, Ecological, Geological and Geophysical Engineering*, Vol. 9, No. 6, (2015), 658–666.
34. Zhu, Y., Chen, G., Chen, Q., Zhang, G., and Shi, Q., "Simulation of material plastic flow driven by non-uniform friction force during friction stir welding and related defect prediction", *Materials & Design*, Vol. 108, (2016), 400–410.
35. Chen, G., Shi, Q., and Zhang, S., "Recent Development and Applications of CFD Simulation for Friction Stir Welding", In: *TMS Annual Meeting & Exhibition*, Springer, Cham, (2018), 113–118.
36. Kim, S.-D., Yoon, J.Y., and Na, S.J., "A study on the characteristics of FSW tool shapes based on CFD analysis", *Welding in the World*, Vol. 61, No. 5, (2017), 915–926.
37. Dialami, N., Chiumenti, M., Cervera, M., and Agelet de Saracibar, C., "Challenges in Thermo-mechanical Analysis of Friction Stir Welding Processes", *Archives of Computational Methods in Engineering*, Vol. 24, No. 1, (2017), 189–225.
38. Gadakh, V.S., and Adepu, K., "Heat generation model for taper cylindrical pin profile in FSW", *Journal of Materials Research and Technology*, Vol. 2, No. 4, (2013), 370–375.
39. Querin, J., and Schneider, J., "Developing an alternative heat indexing equation for FSW", *Welding Journal*, Vol. 91, (2012), 76–82.
40. Xiao, Y., Zhan, H., Gu, Y., and Li, Q., "Modeling heat transfer during friction stir welding using a meshless particle method", *International Journal of Heat and Mass Transfer*, Vol. 104, (2017), 288–300.
41. Dialami, N., Cervera, M., Chiumenti, M., Segatori, A., and Osikowicz, W., "Experimental Validation of an FSW Model with an Enhanced Friction Law: Application to a Threaded Cylindrical Pin Tool", *Metals*, Vol. 7, No. 11, (2017), 491–504.
42. Avila, J.A., Giorjao, R.A.R., Rodriguez, J., Fonseca, E.B., and Ramirez, A.J., "Modeling of thermal cycles and microstructural analysis of pipeline steels processed by friction stir processing", *The International Journal of Advanced Manufacturing Technology*, Vol. 98, No. 9–12, (2018), 2611–2618.
43. Unfried-Silgado, J., Torres-Ardila, A., Carrasco-García, J.C., and Rodríguez-Fernández, J., "Effects of shoulder geometry of tool on microstructure and mechanical properties of friction stir welded joints of AA1100 aluminum alloy", *DYNA*, Vol. 84, No. 200, (2017), 202–208.
44. Hamilton, R., MacKenzie, D., and Li, H., "Multi-physics

- simulation of friction stir welding process”, *Engineering Computations*, Vol. 27, No. 8, (2010), 967–985.
45. Shi, Q.Y., Chen, G.Q., Wang, X.B., and Kang, X., “Numerical Analysis of Multi-Field Coupled Phenomena in Friction Stir Welding and Applications”, *Materials Science Forum*, Vol. 783–786, (2014), 1794–1807.
  46. Arora, A., Nandan, R., Reynolds, A.P., and DebRoy, T., “Torque, power requirement and stir zone geometry in friction stir welding through modeling and experiments”, *Scripta Materialia*, Vol. 60, No. 1, (2009), 13–16.
  47. Biswas, P., and Mandal, N.R., “Effect of Tool Geometries on Thermal History of FSW of AA1100”, *Welding Journal*, Vol. 90, (2011), 129–135.
  48. Su, P., Gerlich, A., North, T.H., and Bendzsak, G.J., “Material flow during friction stir spot welding”, *Science and Technology of Welding and Joining*, Vol. 11, No. 1, (2006), 61–71.
  49. Nandan, R., Roy, G.G., Lienert, T.J., and Debroy, T., “Three-dimensional heat and material flow during friction stir welding of mild steel”, *Acta Materialia*, Vol. 55, No. 3, (2007), 883–895.
  50. Shi, H., McLaren, A.J., Sellars, C.M., Shahani, R., and Bolingbroke, R., “Constitutive equations for high temperature flow stress of aluminium alloys”, *Materials Science and Technology*, Vol. 13, No. 3, (1997), 210–216.
  51. Das, B., Pal, S., and Bag, S., “Torque based defect detection and weld quality modelling in friction stir welding process”, *Journal of Manufacturing Processes*, Vol. 27, (2017), 8–17.
  52. Song, M., and Kovacevic, R., “Numerical and experimental study of the heat transfer process in friction stir welding”, *Proceedings of the Institution of Mechanical Engineers, Part B: Journal of Engineering Manufacture*, Vol. 217, No. 1, (2003), 73–85.

## A Coupled Rigid-viscoplastic Numerical Modeling for Evaluating Effects of Shoulder Geometry on Friction Stir-welded Aluminum Alloys

J. Fabregas Villegas<sup>a</sup>, A. Martínez Guarín<sup>b</sup>, J. Unfried-Silgado<sup>b</sup>

<sup>a</sup> Departamento de Ingeniería mecánica, Grupo IMTEF, Universidad Autónoma del Caribe, Barranquilla, Colombia

<sup>b</sup> Departamento de Ingeniería mecánica, Grupo ICT, Universidad de Córdoba, Montería, Colombia

### PAPER INFO

### چکیده

#### Paper history:

Received 24 August 2018

Received in revised form 28 October 2018

Accepted 03 January 2019

#### Keywords:

Friction Stir Welding  
Finite Element Model  
Aluminum Alloy  
Heat Generation  
Plasticity

هندسه شانه‌ای از ابزار نقش مهمی در جوشکاری اصطکاک ایفا می‌کند، زیرا کنترل اثر متقابل حرارتی و تولید گرما را کنترل می‌نماید. در این کار، یک مدل‌سازی عددی مشخص و ویسکوپلاستیک با استفاده از دینامیک سیالات محاسباتی و محاسبات عناصر محدود با هدف درک این تعاملات ارائه شده است. مدل حل معادلات حفاظتی جرم، حرکتی و انرژی را در سه بعد، با استفاده از شرایط مرزی مناسب، با توجه به جریان جرم به عنوان مواد غیرنیوتنی، ناپایدار، ویسکوپلاستی. شرایط مرزی انتقال حرارت و جریان مواد با استفاده از یک وضعیت تماس کششی/کششی در رابط ابزار/قطعه کار اندازه‌گیری شد. تاریخچه حرارتی، همچنین تنش برشی و میدان‌های سرعت چرخشی، نیروها و مقادیر گشتاور برای سه حالت هندسی شانه محاسبه شده است. نتایج عددی تاریخ حرارتی، گشتاور و نیروها در طی جوشکاری همبستگی خوب با داده‌های آزمایش شده را نشان می‌دهد.

doi: 10.5829/ije.2019.32.02b.17